Soft Matter

Local Changes in Protein Filament Properties Drive Large-Scale Membrane Transformations Involved in Endosome Tethering and Fusion

Journal:	*Soft Matter*
Manuscript ID	SM-ART-03-2024-000299.R1
Article Type:	Paper
Date Submitted by the Author:	16-May-2024
Complete List of Authors:	Ghosh, Ashesh; Stanford University, Chemical Engineering; University of California Berkeley, Chemistry Spakowitz, Andrew; Stanford University, Chemical Engineering

Soft Matter

ARTICLE TYPE

Cite this: DOI: 00.0000/xxxxxxxxxx

Local Changes in Protein Filament Properties Drive Large-Scale Membrane Transformations Involved in Endosome Tethering and Fusion

Ashesh Ghosh,[a‡] Andrew J. Spakowitz,[a,b,c]

Received Date
Accepted Date

DOI: 00.0000/xxxxxxxxxx

Large-scale cellular transformations are triggered by subtle physical and structural changes to individual biomacromolecular and membrane components. A prototypical example of such an event is the orchestrated fusion of membranes within an endosome that enables transport of cargo and processing of biochemical moieties. In this work, we demonstrate how protein filaments on the endosomal membrane surface can leverage a rigid-to-flexible transformation to elicit a large-scale change in membrane flexibility to enable membrane fusion. We develop a polymer field-theoretic model that captures molecular alignment arising from nematic interactions with varying surface density and fraction of flexible filaments, which are biologically controlled within the endosomal membrane. We then predict the collective elasticity of the filament brush in response to changes in the filament alignment, predicting a greater than 20-fold increase of the effective membrane elasticity over the bare membrane elasticity that is triggered by filament alignment. These results show that the endosome can modulate the filament properties to orchestrate membrane fluidization that facilitates vesicle fusion, providing an example of how active processes that modulate local molecular properties can result in large-scale transformations that are essential to cellular survival.

1 Introduction

Cellular self-organization and large-scale orchestrated transformations are driven by coordinated biophysical, mechanical, and dynamical processes involving numerous biomacromolecules and biological membranes. A fundamental challenge in understanding and predicting cellular self-organization and dynamics stems from the need to determine how molecular components (*e.g.* RNA, proteins, lipids) leverage subtle physical changes to drive dramatic cellular transformations across different length and time scales [1,2,3,4]. The complex interplay of microscopic chemical events in membranes, including lipid-raft formation [5], coupled lipid-protein interactions [6], dynamin-driven membrane fission [7], clathrin-mediated endocytosis [8,9], and active transport of fluid across membranes [10,11], determine critical biological fates such as cell shape and function [12]. Studies show membrane protein interactions and protein absorption can alter the local curvature of a membrane and consequential for endocytosis, vesiculation and tubulation [13,14]. Coordinated membrane fusion enables the transport of critical cargo and biochemicals to and from the cell [15], which is an essential biological process involving subtle biophysical events.

In this work, we develop a theoretical model for the physical transformations in the endosomal membrane that underlie membrane fusion and transport, which serves as a prototypical example of cellular self-organization and dynamics. Recently, allosteric changes to the early endosome tether protein EEA1 (Fig. 1) has been shown to play an important role in mechanical pulling of membranes to close spatial proximity upon binding with a vesicle bearing small GTPase Rab5 in its GTP bound form Rab5(GTP). EEA1 is a coiled-coil dimeric molecule with a contour length of $L \sim 222 \pm 26$ nm and a persistence length of $l_p^{\mathrm{EEA1}} \sim 246 \pm 42$ nm. EEA1 predominantly exists in "extended" or rigid conformation (Fig. 1A) in its free N-terminus unbound form [16]. Upon binding to Rab5(GTP) the contour length essentially remains the same. However, the molecule shifts to a more "flexible" conformation (Fig. 1B) with an average end-to-end distance of $\sim 122 \pm 50$ nm, coinciding with a persistence length of $l_p^{\mathrm{EEA1(GTP)}} \sim 74 \pm 3$ nm [16].

Changes in the population density of the structurally rigid (or flexible) EEA1 filaments is thought to play a crucial role in mechanical pulling of membranes via thermal and active enzymatic fluctuations present in the cellular media. Moreover, EEA1 is present in high density patches on the membrane surface and thus forms a switchable polymer brush layer [17]. It is to be noted that

[a] *Department of Chemical Engineering, Stanford University*
[b] *Biophysics Program, Stanford University*
[c] *Department of Materials Science & Engineering, Stanford University, Stanford, CA 94305, email: ajspakow@stanford.edu*
‡ Present address: Department of Chemistry and Chemical Engineering, University of California Berkeley, CA 94720.

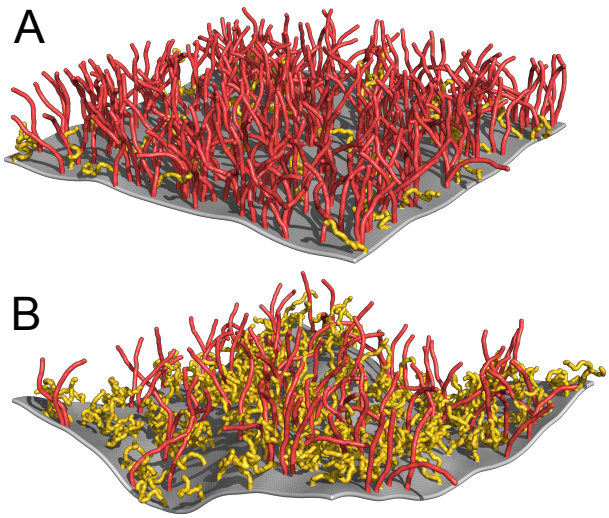

Fig. 1 Schematic of an endosomal membrane with EEA1 brush layer. The A and B images show the collective behavior of the brush layer in the predominantly extended and predominantly collapsed states on the surface of a patch of elastic membrane. Yellow and Red colored polymers are in the collapsed flexible and extended rigid conformations, respectively. The effective elastic rigidity of the membrane and brush is higher in the aligned state of polymer brush layer (panel A). Molecular-level changes that transform polymers from extended to flexible conformation (red → yellow) alter membrane rigidity and induce large length-scale fluctuations.

such a structure-driven entropic transition is not unique to EEA1-tether system, but common in coil-coiled tether proteins, such as GCC185 that binds to Rab9(GTP)[18]. Hence, these long coil-coiled tethers can act as a mechanical switch in bringing distant membranes to physical proximity to facilitate fusion[16,19].

Our work develops a molecular-level model that captures the collective alignment within an EEA1 brush with varying fractions of flexible and rigid protein filaments. Furthermore, we provide a prediction for how the collective brush layer alters the effective elasticity of the membrane and makes it more susceptible for fusion. More concretely, we construct a general thermodynamic model of two types of semiflexible polymers in a solvent and specialize to our case to determine how nematic interactions that originate from hydrophobic moieties along the chain backbone of coil-coiled proteins dictate chain alignment and alter the collective membrane rigidity. The properties and phenomena focus on molecular alignment within EEA1 tethered system. Furthermore, this work provides fundamental insight into how the cell can control molecular properties of specific biomacromolecules to elicit large-scale transformations involved in major biological events.

2 Model and Theory

We consider an incompressible polymer solution of total volume V, with n_s solvent molecules with molecular volume v_s, n_p^R rigid polymer chains with contour length L_R and cross-sectional area A_R and n_p^F flexible polymer chains with contour length L_F and cross-sectional area A_F. The polymer chains are modeled using the wormlike chain model, which describes the polymer chains as inextensible elastic threads that are subjected to thermal fluctuations[20,21]. The polymer configuration of the ith polymer of type $\alpha \in [R,F]$ at arc-length position s (note, $s=0$ at one end and $s=L_\alpha$ at the opposite end) is defined by the space curve $\vec{r}_i^{\,\alpha}(s)$, and the local tangent vector $\vec{u}_i^{\,\alpha}(s) = \partial \vec{r}_i^{\,\alpha}(s)/\partial s$ gives the tangent orientation of the monomer segment at s. Here and in the following discussion, the index α indicates the polymer species, where R and F signify rigid and flexible polymer types, respectively. Inextensibility is strictly enforced by ensuring that $|\vec{u}_i^{\,\alpha}(s)| = 1$ for all configurations of the system. The position of the jth solvent molecule is given by $\vec{r}_j$. The bending rigidity of the semiflexible polymers are given by their respective persistence lengths l_p^α, and we also express the chain length in dimensionless units as the number of Kuhn lengths $N_\alpha = L_\alpha/b_\alpha$, where the Kuhn length $b_\alpha = 2l_p^\alpha$ gives the statistical segment length of a polymer.

The system energy includes contributions for polymer bending deformation, solvent-polymer mixing enthalpy captured through effective Flory-Huggins χ-parameters[22], and nematic alignment free energy of polymer chains through an effective Maier-Saupe interaction[23,24]. The total energy is given by

$$\begin{aligned}\beta E = \sum_{\alpha\in[R,F]} \Bigg\{ \sum_{i=1}^{n_p^\alpha} \frac{l_p^\alpha}{2} \int_0^{L_\alpha} ds \left(\frac{\partial \vec{u}_i^{\,\alpha}(s)}{\partial s}\right)^2 \\ + \chi_\alpha \int d\vec{r}\, \hat{\phi}_s(\vec{r})\hat{\phi}_p^\alpha(\vec{r}) - \frac{a_\alpha}{2}\int d\vec{r}\, \hat{\mathbf{S}}_\alpha(\vec{r}) : \hat{\mathbf{S}}_\alpha(\vec{r}) \Bigg\} \\ + \chi_{RF} \int d\vec{r}\, \hat{\phi}_p^R(\vec{r})\hat{\phi}_p^F(\vec{r}) - a_{RF}\int d\vec{r}\, \hat{\mathbf{S}}_R(\vec{r}) : \hat{\mathbf{S}}_F(\vec{r}), \end{aligned} \quad (1)$$

where $\hat{\phi}_s(\vec{r})$ and $\hat{\phi}_p^\alpha(\vec{r})$ respectively define the local dimensionless density (volume fraction) of the solvent and polymer molecules of type α at spatial location $\vec{r}$, and $\hat{\mathbf{S}}_\alpha(\vec{r})$ is the tensorial nematic order parameter density of state α at $\vec{r}$[25,26,27]. Defining a generalized volume fraction in terms of real spherical harmonics[28] allows us to write the thermodynamic energy in a consolidated form as done in Ref.[25] for a one-component polymer system (details in Appendix, sec. 5.1-5.4). Specifically this allows us to represent both the scalar volume fraction and the tensorial nematic order-parameter field using the same level of description in terms of spherical-harmonic weighted density fields. In the appendix, we write the canonical partition function $\mathscr{Z}$, followed by a series of standard polymer field-theoretic transformations[22]. Using the saddle-point approximation[22], we write the homogeneous mean-field free energy density, $\beta f_0 \equiv \beta F/V = -V^{-1}\log\mathscr{Z}$ of the system as

$$\begin{aligned}\beta f_0 \;=\; & \frac{1-\phi_p}{v_s}\log(1-\phi_p) + \sum_{\alpha\in[R,F]} \Bigg\{ \frac{\phi_p^\alpha}{L_\alpha A_\alpha}\log\phi_p^\alpha \\ & + \chi_\alpha \phi_p^\alpha(1-\phi_p) - \frac{a_\alpha}{3}(\phi_p^\alpha)^2 m_\alpha^2 + \frac{\phi_p^\alpha}{L_\alpha A_\alpha}\log q_\alpha \Bigg\} \\ & + \chi_{RF}\phi_p^R\phi_p^F - \frac{2a_{RF}}{3}\phi_p^R\phi_p^F m_R m_F, \end{aligned} \quad (2)$$

where ϕ_p^α is the bulk volume fraction of polymer α ($\alpha \equiv$ species

index), and the total polymer volume fraction is $\phi_p = \phi_p^R + \phi_p^F$. Conceptually, the nematic order-parameter density $\hat{\mathbf{S}}(\vec{r})$ transforms to the bulk volume fraction ϕ_p multiplied by the nematic order parameter m in the mean-field treatment. The nematic order parameter m_α of polymer type α is defined as $m_\alpha = \frac{1}{L_\alpha}\int_0^{L_\alpha} ds \langle P_2(u_z^\alpha(s))\rangle_{0_\alpha}$ where, $P_2(x) = (3x^2-1)/2$ is the Legendre polynomial of order 2. The precise structure of $P_2(x)$ originates from the equivalence of the Maier-Saupe form of the nematic order parameter and the definition of our generalized volume fraction, since

$$(\vec{u}_1\vec{u}_1 - \mathbf{I}/3)_{ij}(\vec{u}_2\vec{u}_2 - \mathbf{I}/3)_{ij} = \frac{2}{3}\sum_{m=-2}^{2} Y_2^m(\vec{u}_1)Y_2^m(\vec{u}_2)$$
$$= \frac{2}{3}P_2(\vec{u}_1\cdot\vec{u}_2).$$

The average $\langle\ldots\rangle_{0_\alpha}$ is taken with respect to the single-chain mean field energy, defined by

$$\beta\mathscr{E}_0^\alpha = \int_0^{L_\alpha} ds\left\{\frac{l_p^\alpha}{2}\left(\frac{\partial\vec{u}^\alpha(s)}{\partial s}\right)^2 - \gamma_\alpha\left[(u_z^\alpha(s))^2 - \frac{1}{3}\right]\right\}, \qquad (3)$$

where $\gamma_\alpha = (a_\alpha\phi_p^\alpha m_\alpha A_\alpha + a_{RF}\phi_p^\beta m_\beta A_\beta)$ gives the molecular field strength for the α-type polymer (note, if $\alpha = R$ then $\beta = F$ and *vice versa*). The single-chain partition function q_α of polymer α is evaluated from a Boltzmann-weighted sum over all polymer-chain conformations with respect to the mean-field energy $\beta\mathscr{E}_0^\alpha$. We note that in the absence of any molecular quadrupole field interactions ($a\to 0$ and $q\to 1$ limit), Eq. 2 reduces to a multicomponent Flory-Huggins (FH) mean-field theory[22]. This FH free energy corresponds to the isotropic state of the multicomponent system.

In this work, we assume the volume fractions in the isotropic and nematic states are the same in order to model transitions in the filament brush for a fixed membrane surface coverage, and we assume $a_R = a_F = a_{RF} = a$. With these assumptions, we write the Helmholtz free energy of the nematic phase relative to the isotropic phase for the alignment strength $\hat{a} = a\phi_p LA$ to be

$$\beta\Delta f_0 = \frac{\hat{a}}{3}(f_R m_R + f_F m_F)^2 - f_R\log q_R - f_F\log q_F, \qquad (4)$$

where $f_\alpha = \phi_p^\alpha/\phi_p$. The Maier-Saupe parameter $\hat{a}$ should be understood as altering the surface coverage of filaments on the membrane. The stability of the nematic phase is determined by finding the curvature of $\beta\Delta f_0$ with respect to the overall variational parameter, defined through the relation $\langle m\rangle = f_R m_R + f_F m_F$. Finally, we note that the end-to-end distance can be calculated from the tangent correlation functions, similar to Ref.[25,29].

Fluctuations around the mean-field state[22] of the polymer brush layer predict the Frank elastic energies of the system that contribute to the effective membrane bending rigidity. Frank elastic energies provide energetic contributions of the polymer layer with respect to the aligned state in terms of the normal modes of deformation such as bend, twist, and splay[25,30,31]. Considering the Canham-Helfrich Hamiltonian[32,33] using a Monge-Gauge representation[34], we note the following relation in the presence

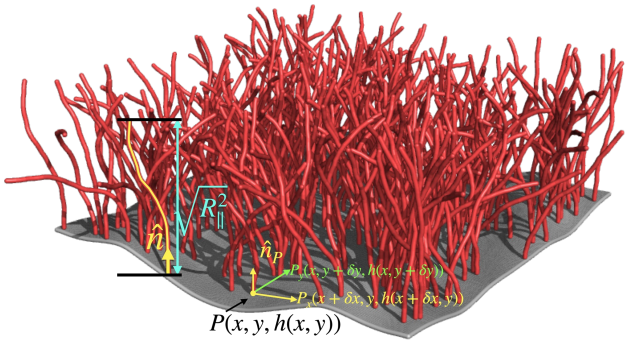

Fig. 2 A membrane patch is shown to schematically show normal at any point on the membrane that holds a polymer. The polymer structural axis is shown in yellow solid line and the polymer end-to-end distance along the preferred direction of alignment in its extended state is shown in cyan double-headed arrow. Construction of unit normal $\hat{n}_P$ at point $P \equiv (x,y,h(x,y))$ is demonstrated as the normalized cross product of $\overrightarrow{PP}_x$ and $\overrightarrow{PP}_y$. The schematic shows defined quantities related to the membrane geometry that are further used in the appendix.

of a polymer brush layer (for details see, Appendix, sec. 5.5):

$$\kappa_{\rm mem}^{\rm eff} = \kappa_{\rm mem} + K_{\rm splay}\sqrt{R_\parallel^2} \geq \kappa_{\rm mem}, \qquad (5)$$

where only the splay modulus $K_{\rm splay}$ is seen to contribute to altering the effective membrane bending modulus, and $R_\parallel^2$ denotes the mean-squared end-to-end distance of the polymer along the nematic alignment direction (schematically shown in Fig. 2). Previous work[35] determines the membrane elasticity to be coupled to the lipid-bilayer splay modulus, which in spirit is similar to what we obtain. However, our single layer membrane elasticity is coupled to splaying of the outer protein-brush layer, and the nematic state of the brush layer becomes crucial for determining the effective membrane rigidity. The stretching modulus of the membrane remains unchanged, since modes of deformation that are affected by the brush layer are associated with directions that are predominantly perpendicular to the in-plane stretching modes. For our case of two different polymers, the effective bending modulus is determined to be the population average $\sim K_{\rm splay}\sqrt{R_\parallel^2}$. Details of a microscopic theory of how fluctuations around the mean-field solution can be used to calculate Frank-elastic constants for semiflexible polymers is given in Ref.[25]. Equation 5 suggests that when $K_{\rm splay} = 0$ in the absence of nematic alignment, the effective membrane elasticity comes from internal rigidity of the lipid bilayer. Hence, thermal (and perhaps active) fluctuations present in the system result in larger height fluctuations of the membrane[36] (*cf.* Fig. 1B). Under conditions of alignment of the polymer molecules, $K_{\rm splay} > 0$, and effective membrane elasticity increases. Physically, this corresponds to suppressed height fluctuations[37] of the membrane due to the extended configurations within the polymer brush layer (*cf.* Fig. 1A).

3 Results and Discussion.

We show results for the two types of polymers with variable dimensionless chain length $N_\alpha = L/2l_p^\alpha$, where the contour length and persistence lengths are set by experimental measurements of EEA1 filaments. This gives the dimensionless chain lengths for

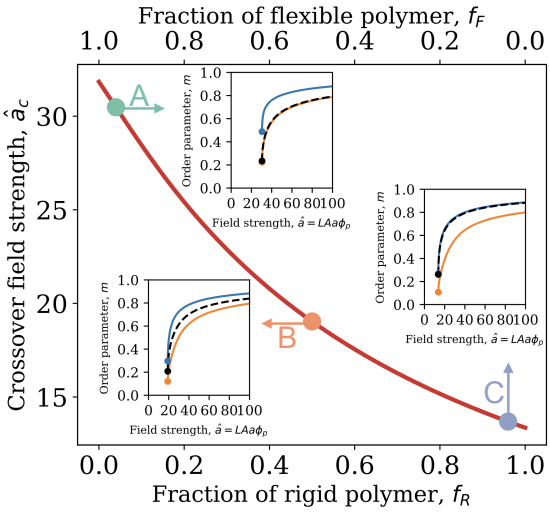

Fig. 3 Critical strength of aligning field as a function of the fraction of rigid polymer (lower X-axis) is plotted. The order parameter variation is shown for three states corresponding to $f_R = 0.04, 0.50$ and 0.96 respectively [blue line is m_R (rigid polymers), orange is m_F (flexible polymers) and the black dashed line follows $\langle m \rangle$].

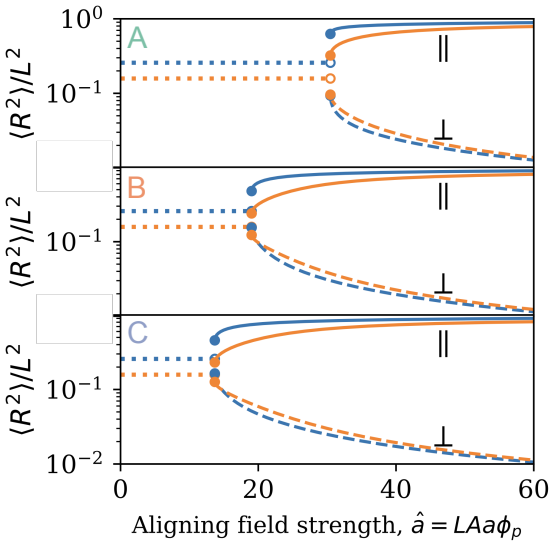

Fig. 4 Mean-squared end-to-end distance normalized by the squared contour length of the polymer chain as a function of aligning field strength for the three states in Fig. 3. Dotted line represents an isotropic state and solid and dashed lines represent $\langle R^2_{\parallel} \rangle$ (along the aligning field) and $\langle R^2_{\perp} \rangle$ ($\perp^r$ to the aligning field) respectively [blue $\equiv$ rigid and orange $\equiv$ flexible].

the rigid and flexible limit to be $N_{\text{rigid}} = 0.50$ and $N_{\text{flexible}} = 1.50$ respectively. The analysis in Ref.[25] suggests $N \leq 10$ demarcates the semiflexible polymer regime for nematic interactions. Hence both the "rigid" and "flexible" structures of EEA1 should be thought of as relatively rigid and relatively flexible cases of semiflexible polymers. We also set all Maier-Saupe parameters a_α to be the same and cross-sectional area is considered to be the same for EEA1 protein in its extended and flexible states. We think of a as an effective parameter (in the same spirit as the effective Flory Higgins parameter χ) that embodies all the complex physical interactions between chains within the polymer brush layer. Hence, the effective alignment strength γ_α depends on the polymer grafting density on a membrane patch, the degree of alignment, and the hydrophobic interactions between chemical groups present on the EEA1 polymer backbone, where increased hydrophobicity leads to increased a. We note that for a fixed composition (i.e. fractions of rigid and flexible polymers) transitioning to a liquid-crystalline phase, the nematic order parameter for the two polymers exhibit a first-order phase transition.

The main plot of Fig. 3 shows the field strength at the nematic transition $\hat{a}_c$ as a function of fraction of rigid polymers f_R. The transition field strength $\hat{a}_c$ systematically decreases with increasing f_R, indicating the system transitions to a nematic state at lower effective strength of alignment interactions. Phase diagrams for the three states [$f_R = 0.04$ (A), 0.50 (B), and 0.96 (C)] showing the nematic order parameters for the flexible and rigid polymers (m_F and m_R, respectively) are given in the inset plots of Fig. 3. The two colors in the inset figures represent m_R (rigid, blue) and m_F (flexible, orange). The population-weighted average nematic order parameter is shown in black dashed line. The limit of stability of the nematic phase $\hat{a}_s$ is shown as the dots in the inset phase diagrams. Both the rigid and flexible polymers exist in the isotropic state with $m_\alpha = 0$ for $a < a_s$. The polymer brush layer exhibits nematic alignment for $a > a_s$, resulting in non-zero nematic ordering for both rigid and flexible polymers.

The isotropic state of the system exhibits orientational symmetry, such that the mean-squared end-to-end distance has equivalent contributions from all directions[25,29]. Upon transitioning to the nematic state, the broken symmetry of correlation lengths along parallel and perpendicular to the field directions result in an 'elongated' polymer along the nematic-director direction[25] (i.e. perpendicular to the membrane). We show the end-to-end distance as a function of aligning field strength for three representative states in Fig. 4. For $\hat{a} < \hat{a}_c$, we obtain a single end-to-end distance in the two directions, and at $\hat{a} = \hat{a}_c$, there is a discontinuous jump associated with elongation along the parallel direction and retraction along the perpendicular direction. With increasing field strength, the polymers become more elongated along the nematic director direction, and perpendicular fluctuations monotonically decrease. The limit of high strength of alignment corresponds to a rigid rod-like state, where the end-to-end distance in the director direction (*cf.* Fig. 2) approaches the contour length of the polymer, *i.e.* $\langle R^2_{\parallel} \rangle \to L^2$.

Within the mean-field approximation, we now consider free energies of the system as given by the purely nematic energy density in Eq. 4. The order parameter of the entire system can be given as $\langle m \rangle$, and variational optimization of the free-energy density as a function of the order parameter gives the optimal value of $\langle m \rangle$ for a particular state. We plot the excess nematic free energy density in Fig. 5A for the three defined states for a fixed $\hat{a} = 27$. As we note from Fig. 3, state A has $\hat{a}_c > 27$, meaning the system would be in isotropic state and variational minimization of free energy predicts the system resides at $\langle m \rangle_0 = 0$, as noted by the circle. For both state B and C, Fig. 3 states $\hat{a}$ should produce a nematic state ($\langle m \rangle_0 > 0$), which is shown in Fig. 5. We note that as the

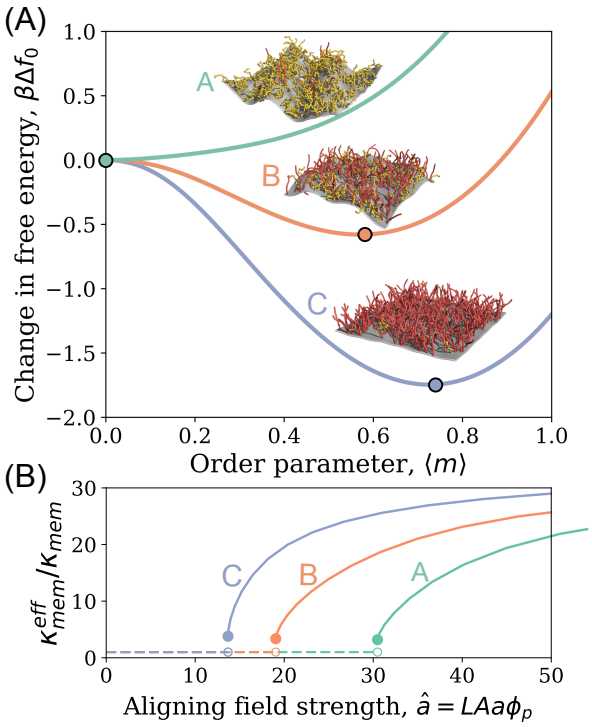

Fig. 5 The top plot (A) shows the change in free energy with respect to the isotropic state is shown as a function of average order parameter variation for the three states of Fig. 3 corresponding to rigid-polymer fractions of 0.04, 0.50 and 0.96 ($A \to B \to C$) for a fixed $\hat{a} = LAa\phi_p = 27$. The bottom plot (B) shows the ratio of effective membrane rigidity as a function of aligning field strength for the three states.

fraction of rigid polymers increase from $A \to B \to C$, $\langle m \rangle_0$ monotonically grows from the isotropic to the nematic state towards $\langle m \rangle_0 \to 1$ indicating perfectly aligned polymer configurations. As the fraction of rigid polymers increase, the nematic free energy of the system decreases indicating stabilizing forces in the system. With the same surface coverage of EEA1 brush-like polymers on a membrane patch, we anticipate a decreasing free energy as the brushes exist in the rigid state.

We assign values of the EEA1 contour length $L = 222$ nm, cross-sectional area $A = 3.1$ nm^2 [17,38], and EEA1 volume fraction $\phi_p = 0.01$ [16,39]. The bare membrane bending elasticity is set to $\kappa_{\rm mem} = 5k_BT$, which is within the measured physiological range [40]. These parameters permit the evaluation of the effective membrane rigidity for the three rigid-polymer fractions shown in Fig. 5A. Figure 5B gives the ratio of the effective membrane rigidity to the bare-membrane rigidity $\kappa^{\rm eff}_{\rm mem}/\kappa_{\rm mem}$ as a function of aligning field strength. For $\hat{a} < \hat{a}_c$ in each state, the effective membrane elasticity $\kappa^{\rm eff}_{\rm mem} = \kappa_{\rm mem}$, since the splay modulus $K_{\rm splay}$ of the filament brush is zero in the isotropic state. At the nematic transition $\hat{a} = \hat{a}_c$, the effective membrane elasticity undergoes a first-order transition associated with the sudden increase in the nematic ordering. Further increase in the aligning field strength leads to a greater than 20-fold increase in the effective elasticity of the membrane and the EEA1 brush, leading to an overall picture where filament alignment dramatically modulates the membrane elasticity.

Notably, this dramatic change in the effective membrane elasticity is enabled by the collective nematic transition. The persistence lengths of the rigid and flexible states have a ratio of $l_p^{\rm EEA1}/l_p^{\rm EEA1(GTP)} \approx 3.3$, indicating a limiting ability for a single filament to physically manipulate exterior cargo. However, the collective elastic behavior of the EEA1 brush would facilitate large-scale property changes that facilitate large deformations of the membrane necessary for membrane fusion.

4 Conclusion

In conclusion, we provide a theoretical model for collective transitions in the EEA1 brush on an endosomal membrane, and our analyses reveal how large-scale membrane fluctuations that are essential for membrane fusion are controlled by subtle physical and structural changes of the molecular constituents. Our work suggests a possible mechanism of membrane fusion that relies on membrane fluidity (or reduced mechanical rigidity), which is modulated by the brush-layer protein filaments. Extended EEA1 molecules that behave as effective rod-like polymers, increases the effective elastic rigidity of membrane through their collective alignment within the protein brush. Conformational changes of EEA1 molecules (from a rigid to a flexible, floppy state) help physical proximity due to less steric hindrance and reduces the mechanical rigidity, allowing fusion to take place.

Further experimental studies to understand and characterize the grafting density of EEA1 on a membrane patch, the fraction of rigid and flexible states in a region of the membrane, role of the Rab5 concentration and interactions between the two polymer strands in EEA1 helix in rigid and flexible states are needed to crucially identify the parameter space of effective nematic interaction between the brush layer. Nevertheless, the qualitative predictions suggest dramatic changes in membrane rigidity that can essentially "solidify" a membrane with small change in the effective interaction or fraction of rigid vs. flexible polymers.

Our theoretical model and subsequent analyses addresses the role the coil-coiled dimeric structure of EEA1 protein in the mechanics of the rigid-flexible transition, kinetics of Rab5-GTP binding, ATP→ADP hydrolysis and Rab5-GDP unbinding, and the molecular mechanisms that are responsible for rigid-to-flexible conformational change. Our results have broad impact beyond the membrane-fusion problem. The model demonstrates how biophysical processes that happen on large, collective length and time scales can originate from orchestrated chemical and physical events at much finer scales, which is a general principle that underlies a range of critical life processes.

5 APPENDIX

5.1 Detailed Derivation of the Polymer Field Theory of a three component polymer nematic solution

5.1.1 System Definition

We consider an incompressible polymer solution of total volume V, with n_s solvent molecule with volume v_s, n_p^R polymer chains with contour length L_R and cross-sectional area A_R and n_p^F polymer chains with contour length L_F and cross-sectional area A_F. The polymer chains are modeled using the wormlike chain model,

which describes the polymer chains as inextensible elastic threads that are subjected to thermal fluctuations. The polymer configuration of the i_αth polymer of type $\alpha \in [R,F]$ at arclength position s (note, $s=0$ at one end and $s=L_\alpha$ at the opposite end) is defined by the space curve $\vec{r}_i^{\,\alpha}(s)$, and the local tangent vector $\vec{u}_i^{\,\alpha}(s) = \partial \vec{r}_i^{\,\alpha}(s)/\partial s$ gives the orientation of the monomer segment at s. Inextensibility is strictly enforced by ensuring that $|\vec{u}_i^{\,\alpha}(s)| = 1$ for all configurations of the system. The position of the jth solvent molecule is given by $\vec{r}_j$. The bending rigidity of the semiflexible polymers are given by their respective persistence lengths l_p^α, and we also express the chain length in dimensionless units as the number of Kuhn lengths $N_\alpha = L_\alpha/b_\alpha$, where the Kuhn length $b_\alpha = 2l_p^\alpha$ gives the statistical segment length of a polymer.

The system energy includes contributions for polymer deformation, solvent-polymer mixing, and nematic alignment of polymer chains and is given by the total energy,

$$\begin{aligned}\beta E = \sum_{\alpha\in[R,F]} \Bigg\{ \sum_{i=1}^{n_p^\alpha} \frac{l_p^\alpha}{2} \int_0^{L_\alpha} ds \left(\frac{\partial \vec{u}_i^{\,\alpha}(s)}{\partial s} \right)^2 + \chi_\alpha \int d\vec{r}\, \hat{\phi}_s(\vec{r}) \hat{\phi}_p^\alpha(\vec{r}) \\ - \frac{a_\alpha}{2} \int d\vec{r}\, \hat{\mathbf{S}}_\alpha(\vec{r}) : \hat{\mathbf{S}}_\alpha(\vec{r}) \Bigg\} \\ + \chi_{RF} \int d\vec{r}\, \hat{\phi}_p^R(\vec{r}) \hat{\phi}_p^F(\vec{r}) - a_{RF} \int d\vec{r}\, \hat{\mathbf{S}}_R(\vec{r}) : \hat{\mathbf{S}}_F(\vec{r}), \quad (6)\end{aligned}$$

where $\hat{\phi}_s$ and $\hat{\phi}_p^\alpha$ are respectively the local dimensionless density (volume fraction) of the solvent and polymer molecules of type α, and $\hat{\mathbf{S}}_\alpha$ is the tensorial nematic order parameter density of state α. These local order parameters are given by

$$\hat{\phi}_s(\vec{r}) = v_s \sum_{j=1}^{n_s} \delta(\vec{r} - \vec{r}_j) \quad (7)$$

$$\hat{\phi}_p^\alpha(\vec{r}) = A_\alpha \sum_{i=1}^{n_p^\alpha} \int_0^{L_\alpha} ds \delta(\vec{r} - \vec{r}_i^{\,\alpha}(s)) \quad (8)$$

$$\hat{S}_\alpha(\vec{r}) = A_\alpha \sum_{i=1}^{n_p^\alpha} \int_0^{L_\alpha} ds \delta(\vec{r} - \vec{r}_i^{\,\alpha}(s)) \left(\vec{u}_i^{\,\alpha}(s) \vec{u}_i^{\,\alpha}(s) - \frac{\mathbf{I}}{3} \right). \quad (9)$$

For the subsequent analyses, we define a generalized volume fraction (tensor) that incorporates local orientational order, defined as[25]

$$\hat{\phi}_{l_\alpha,m_\alpha}(\vec{r}) = A_\alpha \sqrt{\frac{4\pi}{2l_\alpha+1}} \sum_{i=1}^{n_p^\alpha} \int_0^{L_\alpha} ds \mathscr{Y}_{l_\alpha}^{m_\alpha}(\vec{u}_i^{\,\alpha}(s)) \delta(\vec{r} - \vec{r}_i^{\,\alpha}(s)). \quad (10)$$

$\mathscr{Y}_{l_\alpha}^{m_\alpha}$ is the real-valued spherical harmonic (i.e. the tesseral spherical harmonic) for state α, given by,

$$\mathscr{Y}_{l_\alpha}^{m_\alpha} = \begin{cases} \sqrt{2}(-1)^{m_\alpha} \mathrm{Im}\left[Y_{l_\alpha}^{|m_\alpha|} \right] & \text{for } m_\alpha < 0 \\ Y_{l_\alpha}^0 & \text{for } m_\alpha = 0 \\ \sqrt{2}(-1)^{m_\alpha} \mathrm{Re}\left[Y_{l_\alpha}^{m_\alpha} \right] & \text{for } m_\alpha > 0 \end{cases} \quad (11)$$

where $Y_{l_\alpha}^{m_\alpha}$ is the standard spherical harmonic (complex valued).

We note that the polymer volume fraction $\hat{\phi}_p^\alpha = \hat{\phi}_{0,0}^\alpha$, and the nematic order parameter $\hat{\mathbf{S}}_\alpha$ can be written in terms of $\hat{\phi}_2^{m_\alpha}$. Details are provided in Ref.[25]. With this definition, we rewrite the system energy as

$$\begin{aligned}\beta E = \sum_{\alpha\in[R,F]} \Bigg\{ \sum_{i=1}^{n_p^\alpha} \frac{l_p^\alpha}{2} \int_0^{L_\alpha} \left(\frac{\partial \vec{u}_i^{\,\alpha}}{\partial s} \right)^2 ds + \chi_\alpha \int d\vec{r}\, \hat{\phi}_s(\vec{r}) \hat{\phi}_{0,0}^\alpha(\vec{r}) \\ - \frac{a_\alpha}{3} \int d\vec{r} \sum_{m=-2}^{2} \left[\hat{\phi}_{2,m}^\alpha(\vec{r}) \right]^2 \Bigg\} + \chi_{AB} \int d\vec{r}\, \hat{\phi}_{0,0}^R(\vec{r}) \hat{\phi}_{0,0}^F(\vec{r}) \\ - \frac{2a_{RF}}{3} \int d\vec{r} \sum_{m=-2}^{2} \hat{\phi}_{2,m}^R(\vec{r}) \hat{\phi}_{2,m}^F(\vec{r}) \quad (12)\end{aligned}$$

where the integrand in the last term in Eq. 12 signifies summation over terms such as, $\hat{\phi}_2^{-2_A}(\vec{r})\hat{\phi}_2^{-2_B}(\vec{r})$, $\hat{\phi}_2^{-1_A}(\vec{r})\hat{\phi}_2^{-1_B}(\vec{r}), \ldots$ and so on.

The canonical partition function, $\mathscr{Z}$ is written as,

$$\begin{aligned}\mathscr{Z} = \frac{1}{n_s! n_p^R! n_p^F!} \frac{1}{v_s^{n_s}} \frac{1}{(L_R A_R)^{n_p^R} (L_F A_F)^{n_p^F}} \\ \times \int \prod_{j=1}^{n_s} d\vec{r}_j \int \prod_{i_A=1}^{n_p^R} \mathscr{D}[\vec{r}_i^{\,R}] \int \prod_{i_F=1}^{n_p^F} \mathscr{D}[\vec{r}_i^{\,F}] \prod_{\vec{r}} \delta(\hat{\phi}_s + \hat{\phi}_{0,0}^R + \hat{\phi}_{0,0}^F - 1) \\ \times \prod_{i_R=1}^{n_p^R} \prod_{i_F=1}^{n_p^F} \prod_{s_R,s_F} \delta(|\partial_{s_R} \vec{r}_i^{\,R}| - 1) \delta(|\partial_{s_F} \vec{r}_i^{\,F}| - 1) \exp(-\beta E) \quad (13)\end{aligned}$$

where $\prod_{\vec{r}} \delta(\hat{\phi}_s + \hat{\phi}_{0,0}^R + \hat{\phi}_{0,0}^F - 1)$ accounts for the incompressibility constraint at all locations within the system. The inextensibility of each polymer chain is enforced by the constraints $\delta(|\partial_{s_\alpha} \vec{r}_i^{\,\alpha}| - 1)$. The integration over $\mathscr{D}[\vec{r}_i^{\,\alpha}]$ implies path integration over all conformations of the polymer α. We use the solvent volume v_s and polymer volume $L_\alpha A_\alpha$ as volume scales instead of the de-Broglie wavelengths cubed, which merely shifts the chemical potential by a constant quantity and does not affect the thermodynamic behavior of our system.

5.1.2 Particle to Field Transformation

Next, we perform a series of field manipulations that enable systematic approximation of the thermodynamic behavior. For each instantaneous volume fraction $\hat{\phi}$, we introduce a volume-fraction field variable by noting the property[25,41]

$$\begin{aligned} f[\hat{\phi}] &= \int \mathscr{D}\phi \prod_{\vec{r}} \delta[\phi - \hat{\phi}] f[\phi] \quad (14) \\ &= \int \mathscr{D}W \mathscr{D}\phi \exp\left\{ i \int d\vec{r}\, W(\vec{r}) \left[\hat{\phi}(\vec{r}) - \phi(\vec{r}) \right] \right\} f[\phi], \end{aligned}$$

where W emerges from a Fourier representation of the spatial delta function. This field manipulation is applied to each volume-fraction ($\hat{\phi}_s$, $\hat{\phi}_{0,0}^\alpha$, and $\hat{\phi}_{2,m}^\alpha$), resulting in the introduction of the conjugate fields W_s, $W_{0,0}^\alpha$, and $W_{2,m}^\alpha$. After these field manipulations, we can write the canonical partition function as,

$$\mathscr{Z} = \int \mathscr{D}W_s \prod_{\alpha\in[R,F]} \left\{ \mathscr{D}\phi^\alpha_{0,0}\mathscr{D}W^\alpha_{0,0} \prod_{m=-2}^{2} \mathscr{D}W^\alpha_{2,m}\mathscr{D}\phi^\alpha_{2,m} \right\} \exp\left\{ i\int d\vec{r} W_s(1-\phi^R_{0,0}-\phi^F_{0,0}) + i\int d\vec{r} \sum_{\alpha\in[R,F]} W^\alpha_{0,0}\phi^\alpha_{0,0} \right.$$

$$+i\int d\vec{r} \sum_{\alpha\in[R,F]}\sum_{m=-2}^{2} W^\alpha_{2,m}\phi^\alpha_{2,m} - \sum_{\alpha\in[R,F]} \chi_\alpha \int d\vec{r}\,\phi^\alpha_{0,0}(1-\phi^R_{0,0}-\phi^F_{0,0}) + \sum_{\alpha\in[R,F]} \frac{a_\alpha}{3}\int d\vec{r} \sum_{m=-2}^{2} \left(\phi^\alpha_{2,m}\right)^2$$

$$\left. -\chi_{RF}\int d\vec{r}\,\phi^R_{0,0}\phi^F_{0,0} + \frac{2a_{RF}}{3}\int d\vec{r} \sum_{m=-2}^{2} \phi^R_{2,m}\phi^F_{2,m} + n_s \log\left(\frac{z_s[W_s]}{n_s v_s}\right) + \sum_{\alpha\in[R,F]} n^\alpha_p \log\left(\frac{z^\alpha_p[W^\alpha_{0,0},W^\alpha_{2,m}]}{n^\alpha_p L_\alpha A_\alpha}\right) \right\} \tag{15}$$

$$= \int \mathscr{D}W_s \prod_{\alpha\in(A,B)} \left\{ \mathscr{D}\phi^\alpha_{0,0}\mathscr{D}W^\alpha_{0,0} \prod_{m=-2}^{2} \mathscr{D}W^\alpha_{2,m}\mathscr{D}\phi^\alpha_{2,m} \right\} \exp\left[-\beta\mathscr{F}\right] \tag{16}$$

where we define the single solvent partition function as

$$z_s[W_s] = \int d\vec{r} \exp\left[-iv_s W_s(\vec{r})\right] \tag{17}$$

and the single polymer partition functions are written as,

$$z^\alpha_p[W^\alpha_{0,0},W^\alpha_{2,m}] = \int \mathscr{D}[\vec{r}^\alpha(s)] \exp\left\{ -\frac{l^\alpha_p}{2}\int_0^{L_\alpha} \left(\frac{\partial\vec{u}_\alpha}{\partial s}\right)^2 ds \right.$$

$$-iA_\alpha \int_0^{L_\alpha} ds W^\alpha_{0,0}(\vec{r}(s))$$

$$\left. -iA_\alpha \int_0^{L_\alpha} ds \sum_{m_\alpha=-2}^{2} W^\alpha_{2,m}(\vec{r}(s))\sqrt{\frac{4\pi}{5}}\mathscr{Y}^m_2(\vec{u_\alpha}(s)) \right\} \tag{18}$$

The partition function $\mathscr{Z}$ has not been subjected to any approximations so far and is not exactly solvable as it is, although it is amenable to systematic approximations. Below we formulate the general saddle-point approximation, which determines the thermodynamic state within a mean-field (generally inhomogeneous) and specialize to the homogeneous mean-field approximation.

5.2 Mean Field Approximation

5.2.1 Mean Field Equations

The lowest-order approximation to the canonical partition function is given by the saddle point, which approximates the functional integrals in Eq. 16 by the maximum term. By setting the first variation of the argument of the exponential within Eq. 16 to zero (i.e. $\frac{\delta(\beta\mathscr{F})}{\delta f} = 0$ for any arbitrary field f), we arrive at the saddle-point equations. We define $\bar{\phi}^\alpha_{0,0} = \phi^\alpha_p$ and $iW = w$ for use in the subsequent analyses. The saddle point equations are given as

$$(1-\phi^R_p-\phi^F_p) = \frac{v_s n_s}{\bar{z}_s}\exp(-v_s\bar{w}_s), \tag{19}$$

$$-\chi_R(1-2\phi^R_p-\phi^F_p) + \chi_F\phi^F_p + \bar{w}^R_{0,0} - \bar{w}_s - \chi_{RF}\phi^F_p = 0, \tag{20}$$

$$-\chi_F(1-\phi^R_p-2\phi^F_p) + \chi_R\phi^R_p + \bar{w}^F_{0,0} - \bar{w}_s - \chi_{RF}\phi^R_p = 0, \tag{21}$$

$$\frac{2a_R}{3}\bar{\phi}^R_{2,m} + \frac{2a_{RF}}{3}\bar{\phi}^F_{2,0} + \bar{w}^R_{2,m} = 0 \tag{22}$$

$$\frac{2a_F}{3}\bar{\phi}^F_{2,m} + \frac{2a_{RF}}{3}\bar{\phi}^R_{2,m} + \bar{w}^F_{2,m} = 0 \tag{23}$$

$$\bar{\phi}^R_p + \frac{n^R_p}{\bar{z}^R_p}\frac{\delta\bar{z}^R_p}{\delta\bar{w}^R_{0,0}} = 0 \tag{24}$$

$$\bar{\phi}^F_p + \frac{n^F_p}{\bar{z}^F_p}\frac{\delta\bar{z}^F_p}{\delta\bar{w}^F_{0,0}} = 0 \tag{25}$$

$$\bar{\phi}^R_{2,m} + \frac{n^R_p}{\bar{z}^R_p}\frac{\delta\bar{z}^R_p}{\delta\bar{w}^R_{2,m}} = 0 \tag{26}$$

$$\bar{\phi}^F_{2,m} + \frac{n^F_p}{\bar{z}^F_p}\frac{\delta\bar{z}^F_p}{\delta\bar{w}^F_{2,m}} = 0 \tag{27}$$

Next, we specialize our treatment of the saddle point to the homogeneous uniaxial nematic state with nematic alignment along $\hat{\delta}_z$. This gives $\bar{\phi}^\alpha_{2,m} = 0$ for $m_\alpha \neq 0$ and $\alpha \in [R,F]$. This leads to the self-consistent mean-field equation (for $\alpha \in [R,F]$)

$$\bar{\phi}^{0_\alpha}_2 = \frac{\phi^\alpha_p}{L_\alpha}\int_0^{L_\alpha} ds \left\langle \left(\frac{3}{2}[u^\alpha_z(s)]^2 - \frac{1}{2}\right)\right\rangle_{0_\alpha} = \phi^\alpha_p m^\alpha_N, \tag{28}$$

where the average $\langle\ldots\rangle_{0_\alpha}$ is taken with respect to the single chain mean-field energy

$$\beta\mathscr{E}^\alpha_0 = \frac{l^\alpha_p}{2}\int_0^{L_\alpha} ds \left(\frac{\partial\vec{u}^\alpha(s)}{\partial s}\right)^2 \tag{29}$$

$$-(a_\alpha\phi^\alpha_p m^\alpha_N A_\alpha + a_{RF}\phi^\beta_p m^\beta_N A_\beta)\int_0^{L_\alpha} ds \left\{ [u^\alpha_z(s)]^2 - \frac{1}{3}\right\}$$

From its definition, we have the constraint $-1/2 \leq m^\alpha_N \leq 1$, for $\alpha \in [R,F]$. The overall nematic order of the system can be thought of as the weighted average $m_{\text{total}} = \frac{1}{\phi_p}\sum_\alpha \phi^\alpha_p m^\alpha_N$. For a perfectly aligned state ($m^\alpha_N = 1$), we get $\bar{\phi}_{2,0} = \sum_\alpha \bar{\phi}^\alpha_{2,0} = \sum_\alpha \phi^\alpha_p = \phi_p$.

5.2.2 Homogeneous Mean-field Approximation and System Energy

For a homogeneous, mean-field approximation, the zeroth order energy becomes (per unit volume V) is given by

$$\beta f_0^{\rm IN} = \frac{1-\phi_p}{v_s}\log(1-\phi_p) + \sum_\alpha \frac{\phi_p^\alpha}{L_\alpha A_\alpha}\log\phi_p^\alpha \tag{30}$$

$$+\sum_\alpha \chi_\alpha \phi_p^\alpha(1-\phi_p) - \sum_\alpha \frac{a_\alpha}{3}(\bar{\phi}_{2,0}^\alpha)^2 + \sum_\alpha \frac{\phi_p^\alpha}{L_\alpha A_\alpha}\log q_\alpha$$

$$+\chi_{RF}\phi_p^R\phi_p^F - \frac{2a_{RF}}{3}\bar{\phi}_{2,0}^R\bar{\phi}_{2,0}^F \tag{31}$$

where $f_0 = \mathscr{F}_0/V$ is an intensive property of the system. Here, q_α is the partition function, given as

$$q_\alpha = \int d\vec{u}\int d\vec{u}_0 \int_{\vec{u}_0}^{\vec{u}} \mathscr{D}[\vec{u}(s)]\exp\{-\beta\mathscr{E}_0^\alpha[\vec{u}(s)]\}. \tag{32}$$

The homogeneous isotropic mean-field free energy is given by

$$\begin{aligned}\beta f_0^{\rm I} &= \frac{1-\phi_p}{v_s}\log(1-\phi_p) + \sum_\alpha \frac{\phi_p^\alpha}{L_\alpha A_\alpha}\log(\phi_p^\alpha)\\ &\quad +\sum_\alpha \chi_\alpha\phi_p^\alpha(1-\phi_p) + \chi_{RF}\phi_p^R\phi_p^F.\end{aligned} \tag{33}$$

Here, it should be noted that in the absence of any aligning field [*i.e.* $\gamma_\alpha = (A_\alpha a_\alpha m_N^\alpha \phi_p^\alpha + A_\beta a_{RF} m_N^\beta \phi_p^\beta)$], the orientational partition is unity. Below we simplify to the notation $m_N^\alpha \equiv m_\alpha$.

The residual Helmholtz free energy (density) of the nematic phase relative to the isotropic phase is given by,

$$\begin{aligned}\beta f_{\rm residual} &= \beta f_0^{\rm I} - \beta f_0^{\rm IN}\\ &= \sum_\alpha\left\{\frac{a_\alpha}{3}(\phi_p^\alpha m_\alpha)^2 - \frac{\phi_p^\alpha}{L_\alpha A_\alpha}\log[q_\alpha(m_\alpha)]\right\}\\ &\quad + \frac{2a_{RF}}{3}\phi_p^R m_R \phi_p^F m_F\end{aligned} \tag{34}$$

For a constant $a_\alpha = a$, $L_\alpha = L$, and $A_\alpha = A$, we get the free energy by multiplying with the relevant volume LA/ϕ_p, resulting in the expressions as written in the main manuscript

$$\beta\Delta f_0 = \frac{\hat{a}}{3}(f_R m_R + f_F m_F)^2 - f_R\log q_R - f_F\log q_F \tag{35}$$

where $\hat{a} = a\phi_p LA$ and $f_\alpha = \phi_p^\alpha/\phi_p$. In the limit of $f_R \to 1$ (hence, $f_F \to 0$) the above equation reduces to (superscript '1' represents single type of polymer component),

$$\beta\Delta f_0^{(1)} = \frac{\hat{a}}{3}m^2 - \log q \tag{36}$$

that matches with Ref.[41].

5.3 Fluctuations around mean field solution

Now we specialize to fluctuation effects upto quartic order with respect to the homogeneous mean field basis. The vector of auxiliary variables are defined as, $\mathscr{W} \equiv [W_s, \{\phi_{0,0}^\alpha\}, \{W_{0,0}^\alpha\}, \{\phi_{2,m}^\alpha\}, \{W_{2,m}^\alpha\}]$ (total of 25 terms) and the vector containing all the fluctuations are defined using, $\Delta = [\{\delta\phi_{0,0}^\alpha\}, \{\delta W_{0,0}^\alpha\}, \{\delta\phi_{2,m}^\alpha\}, \{\delta W_{2,m}^\alpha\}]$ (total of 24 terms due to the incompressibility constraint). Performing Gaussian integral over the fluctuating conjugate fields (not volume fraction fluctuation fields), we arrive at,

$$-\beta\mathscr{F} = -\beta\mathscr{F}_0 - \frac{1}{2}\tilde{\Gamma}_{\tilde{1}\tilde{2}}^{(2,\phi)}\Delta_{\tilde{1}}\Delta_{\tilde{2}} + \sum_{n=3}^{\infty}\frac{1}{n!}\tilde{\Gamma}_{\tilde{1}\ldots\tilde{n}}^{(n,\phi)}\Delta_{\tilde{1}}\ldots\Delta_{\tilde{n}} \tag{37}$$

where the above expansion is formally exact and written using modified Einstein notation to sum over fluctuating volume fraction fields of all constituents and integration over the respective Fourier variables. The quadratic order term can be explicitly written as,

$$\tilde{\Gamma}_{\tilde{1}\tilde{2}}^{(2,\phi)}\Delta_{\tilde{1}}\Delta_{\tilde{2}} = \frac{1}{(2\pi)^6}\sum_{\gamma_1,\gamma_2}\int d\vec{k}_1 d\vec{k}_2 \tilde{\Gamma}_{\gamma_1\gamma_2}^{(2,\phi)}(\vec{k}_1,\vec{k}_2)\Delta_{\gamma_1}(\vec{k}_1)\Delta_{\gamma_2}(\vec{k}_2) \tag{38}$$

where γ runs over the three species present in the system (polymer R and polymer F, noting $\delta\phi_s = -\delta\phi_{0,0}^R - \delta\phi_{0,0}^F$) and over the l and m indices (i.e. $l=0$, $m=0$ and $l=2$, $m=-2,\ldots,2$). In order to write the full matrix $\Gamma^{(2,\phi)}$ in terms of its elements, we write the structure factors for polymer species α as

$$S_{(l_1,m_1),(l_2,m_2)}^{(\alpha)}(\vec{k}) = \frac{1}{L_\alpha^2}\left[\frac{4\pi}{(2l_1+1)(2l_2+1)}\right]^{(m_1+m_2)/2} \tag{39}$$

$$\times\int_0^{L_\alpha} ds_1\int_0^{L_\alpha} ds_2\left\langle \mathscr{Y}_{l_1}^{m_1}(\vec{u}(s_1))\exp\left[i\vec{k}\cdot(\vec{r}_1-\vec{r}_2\right]\mathscr{Y}_{l_2}^{m_2}(\vec{u}(s_2))\right\rangle,$$

where $\vec{r}_1 = \vec{r}(s_1)$ and $\vec{r}_2 = \vec{r}(s_2)$. The entire $\Gamma^{(2,\phi)}$ matrix is a 12×12 matrix containing all the volume fraction fluctuations. The matrix is sparse containing only certain non-zero elements ($\beta \neq \alpha$ in equations below and both indicates A and B):

$$\Gamma_{(0,0),(0,0)}^{(\alpha)}(\vec{k}) = \frac{1}{v_s(1-\phi_p)} - 2\chi_\alpha + \frac{1}{A_\alpha L_\alpha\phi_p^\alpha}[S_{(0,0),(0,0)}^{(\alpha)}]^{-1}(\vec{k}) \tag{40}$$

$$\Gamma_{(0,0),(2,m)}^{(\alpha)}(\vec{k}) = \frac{1}{A_\alpha L_\alpha\phi_p^\alpha}[S_{(0,0),(2,m)}^{(\alpha)}]^{-1}(\vec{k}) \tag{41}$$

$$\Gamma_{(2,m_1),(2,m_2)}^{(\alpha)}(\vec{k}) = -\frac{2a_\alpha}{3}\delta_{m_1m_2} + \frac{1}{A_\alpha L_\alpha\phi_p^\alpha}[S_{(2,m_1),(2,m_2)}^{(\alpha)}]^{-1}(\vec{k}) \tag{42}$$

$$\Gamma_{(0,0),(0,0)}^{(\alpha\beta)}(\vec{k}) = -2\chi_{\alpha\beta} \tag{43}$$

$$\Gamma_{(2,m_1),(2,m_2)}^{(\alpha\beta)}(\vec{k}) = -\frac{2a_{\alpha\beta}}{3}\delta_{m_1m_2} \tag{44}$$

To note, these expressions do not exhibit cross correlation of structure between polymers R and F, since they are separate from one another (*i.e* not a copolymer-like architecture). The formulation above gives the exact free energy up to quadratic order.

Next steps involve, (1) writing the quadratic order free energy within the RPA approximation in terms of the eigenvalues of $\Gamma^{(2,\phi)}$ matrix, (2) defining a non-interacting reference free energy, (3) subtract this reference free energy and (4) using the property, $\prod_{\eta\in\{\text{fields}\}}\gamma_\eta = \det[\Gamma]$ (where γ are the eigenvalues of the determinant and the number of eigenvalues are same as the number of fluctuating volume fraction fields) to arrive at

$$\beta\mathscr{F} = \beta\mathscr{F}_0 + \frac{V}{4\pi^2}\int_0^\Lambda dk\, k^2\log\left\{\frac{\det[\Gamma^{(2,\phi)}]}{\det[\Gamma_0^{(2,\phi)}]}\right\} \tag{45}$$

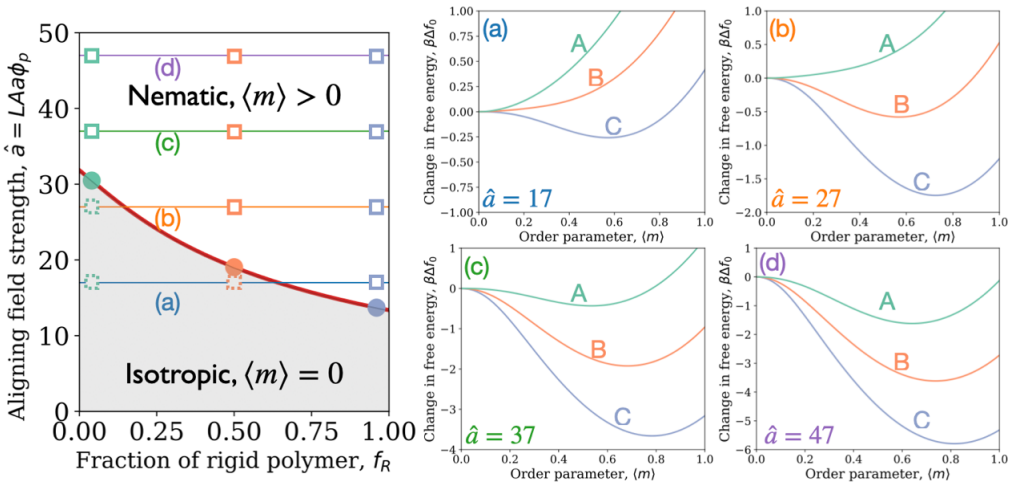

Fig. 6 Phase diagram showing the boundary (thick solid line) of isotropic (gray) and nematic states as a function of rigid polymer fraction, f_R. Figures ((a)-(d)) show changes in free energy (cf. Fig. 5) for state A ($f_R = 0.04$), state B ($f_R = 0.50$) and state C ($f_R = 0.96$) for $\hat{a} = 17, 27, 37, 47$ (panel (a) through (d) respectively). The states that are isotropic are designated as dashed squares in the left phase diagram while the states that shows nematic ordering are shown in solid squares in the phase diagram.

In the above equation, we have introduced a high-k cutoff, $\Lambda = \min_{\{l_p^\alpha\}} \frac{2\pi}{l_p^\alpha}$ to account for the ultraviolet divergence in field theory.

5.4 Chemical potential and system Phase Behavior

We only care about the phase behavior at the mean-field level. Due to enforced incompressibility of the system the Gibbs and Helmholtz free energy of the system are equivalent to one other. Here, we define the chemical potential of η^{th} species as,

$$\beta\mu_\eta = \frac{\partial(\beta\mathscr{F})}{\partial n_\eta} = \beta v_\eta f + V\frac{\partial(\beta f)}{\partial n_\eta} \tag{46}$$

where the second equality follows from defining the free energy density, as $f = \mathscr{F}/V$. The expression for the zeroth order chemical potential of species θ follows from the expression of mean field free energy of the system. We write the mean field energy in a consolidated notation as,

$$\beta f_0 = \sum_k \frac{\phi_k}{v_k}\log\left(\frac{\phi_k}{q_k}\right) + \frac{1}{2}\sum_{j,k}\chi_{jk}\phi_j\phi_k - \frac{1}{3}\sum_{j,k}a_{jk}m_j m_k\phi_j\phi_k \tag{47}$$

$$= \sum_k \frac{\phi_k}{v_k}\log\left(\frac{\phi_k}{q_k}\right) + \frac{1}{2}\sum_{j,k}\Xi_{jk}\phi_j\phi_k \tag{48}$$

where $\Xi_{jk} = \chi_{jk} - \frac{2}{3}a_{jk}m_j m_k$. This leads to the expression for mean field chemical potential for species i as, (where $i \in \{\text{solvent}, \text{polymer } A, \text{polymer } B\}$)

$$\beta\mu_0^{(i)} = 1 + \log\left(\frac{\phi_i}{q_i}\right) - v_i\sum_j\frac{1}{v_j}\phi_j + v_i\sum_j\Xi_{ij}\phi_j - \frac{v_i}{2}\sum_{jk}\Xi_{jk}\phi_j\phi_k \tag{49}$$

where all the ϕ_i denote the mean-field volume fraction of species i.

5.5 Effective Membrane Rigidity

5.5.1 Frank Elastic Energy of Polymer Brush Layer

Here, we briefly describe how existence of polymer brush layer in its extended state is responsible for renormalizing the membrane bending rigidity. Noting that one end of the polymer is tethered to the membrane, we approximate the Frank elastic energy of the polymer brush layer as[25]

$$\beta F_{\text{elas}} = \frac{1}{2}\int d\vec{r}\left[K_{\text{bend}}\left(\vec{n}\times\vec{\nabla}\times\vec{n}\right)^2 + K_{\text{twist}}\left(\vec{n}\cdot\vec{\nabla}\times\vec{n}\right)^2 + K_{\text{splay}}\left(\vec{\nabla}\cdot\vec{n}\right)^2\right] \tag{50}$$

$$\approx \frac{1}{2}\int d\vec{x}\left[K_{\text{bend}}\left(\vec{n}_P\times\vec{\nabla}\times\vec{n}_P\right)^2 + K_{\text{twist}}\left(\vec{n}_P\cdot\vec{\nabla}\times\vec{n}_P\right)^2 + K_{\text{splay}}\left(\vec{\nabla}\cdot\vec{n}_P\right)^2\right]\sqrt{R_\parallel^2} \tag{51}$$

where the 2-dimensional vector $\vec{x} \equiv (x,y)$, and $\vec{n}_P$ is the nematic director direction at polymer leg on the membrane (point P) and couples directly to membrane height fluctuation field. Hence, $\vec{n}_P$ at point P on the membrane can be identified as a normal to the membrane at P. This can be calculated by parametrizing the membrane as $P \equiv (x,y,h(x,y))$, where $h(x,y)$ represents the height of the membrane at $2d$ grid point on the membrane (x,y). Hence, the normal at point P is given by

$$\vec{n}_P = \frac{\overrightarrow{PP}_x \times \overrightarrow{PP}_y}{||\overrightarrow{PP}_x \times \overrightarrow{PP}_y||} = \frac{-h_x\hat{\delta}_x - h_y\hat{\delta}_y + \hat{\delta}_z}{\sqrt{1+h_x^2+h_y^2}} \approx -h_x\hat{\delta}_x - h_y\hat{\delta}_y + \hat{\delta}_z \tag{52}$$

where $h_x = \frac{\partial h(x,y)}{\partial x}$ and the approximate identity gives us variations with respect to minimal order changes in membrane height fluctuations. Looking at the bend and twist terms of Frank elastic

energy we note that, $(\vec{\nabla}\times\vec{n}_P) = h_{zy}\hat{\delta}_x - h_{zx}\hat{\delta}_y$, where $h_{zy} = \dfrac{\partial^2 h(x,y)}{\partial z \partial y}$ and thus are all higher order terms. This implies only splay rigidity of the polymers contribute to the Frank elastic energy to minimal order and is given by

$$\beta F_{\text{elas}} \approx \frac{1}{2} K_{\text{splay}} \sqrt{R_{\parallel}^2} \Big(h_{xx} + h_{yy}\Big)^2 \tag{53}$$

5.5.2 Helfrich Free Energy of Membrane and Renormalized Bending Rigidity

For our case, we consider a membrane with the symmetric distribution of all membrane components (such as lipids and proteins) and the same environment on both sides of the membrane that may ensure symmetric membrane fluctuations and, thereby zero spontaneous curvature. The free energy for such a symmetric membrane is generally expressed as the Helfrich Hamiltonian[32], given as

$$\beta \mathscr{F}[h(\vec{x})] = \int d^2\vec{x} \Big[\frac{\nu_{\text{mem}}}{2} (\vec{\nabla} h(\vec{x}))^2 + \frac{\kappa_{\text{mem}}}{2} (\nabla^2 h(\vec{x}))^2 \Big] \tag{54}$$

where $h(\vec{x})$ describes the height of the membrane at location $\vec{x} \equiv (x,y)$ with respect to a reference state. In the above equation ν_{mem} and κ_{mem} represent the membrane tension and (bending) rigidity respectively. The membrane bending rigidity at any point per above Helfrich Hamiltonian can be written as, $\dfrac{\kappa_{\text{mem}}}{2}(h_{xx} + h_{yy})^2$. Hence the membrane rigidity is renormalized due to Frank elastic energies of polymers and is given by,

$$\kappa_{\text{mem}}^{\text{eff}} = \kappa_{\text{mem}} + K_{\text{splay}} \sqrt{R_{\parallel}^2} \geq \kappa_{\text{mem}} \tag{55}$$

Qualitatively, we can infer in the isotropic state of polymer brush layer, the splay rigidity do not contribute to the overall membrane bending resistance. However, in the nematic extended state of the polymer brush layer, we have finite K_{splay} and effective membrane rigidity increases to larger stiffness prone to lesser fluctuations due to thermal and active forces in the medium. In essence the ratio, $\Theta_{p/m} = K_{\text{splay}} \sqrt{R_{\parallel}^2} / \kappa_{\text{mem}}$ controls membrane fluctuations to zeroth order.

Conflicts of interest

There are no conflicts to declare.

Acknowledgements

A.G. acknowledges funding support from the Human Frontier Science Program, Grant No. HFSP/REF RGP0019/20. A.J.S. was supported by the NSF program Condensed Matter and Materials Theory, Grant No. 1855334.

Notes and references

1 D. McCusker, *Molecular Biology of the Cell*, 2020, **31**, 143–148.
2 N. A. Dye, M. Popović, K. V. Iyer, J. F. Fuhrmann, R. Piscitello-Gómez, S. Eaton and F. Jülicher, *Elife*, 2021, **10**, e57964.
3 P. Recouvreux and P.-F. Lenne, *Current opinion in cell biology*, 2016, **38**, 18–23.
4 S. Furse and G. C. Shearman, *Biochimica et Biophysica Acta (BBA)-Molecular and Cell Biology of Lipids*, 2018, **1863**, 9–19.
5 E. Ikonen, *Current opinion in cell biology*, 2001, **13**, 470–477.
6 M. F. Brown, *Annual review of biophysics*, 2017, **46**, 379–410.
7 M. Pannuzzo, Z. A. McDargh and M. Deserno, *Elife*, 2018, **7**, e39441.
8 J. Hassinger, G. Oster, D. Drubin and P. Rangamani, *Biophysical Journal*, 2017, **112**, 310a.
9 N. Cordella, T. J. Lampo, N. Melosh and A. J. Spakowitz, *Soft matter*, 2015, **11**, 439–448.
10 P. Girard, J. Prost and P. Bassereau, *Physical Review Letters*, 2005, **94**, 088102.
11 C. Wilhelm, *Physical Review Letters*, 2008, **101**, 028101.
12 P. Bassereau, R. Jin, T. Baumgart, M. Deserno, R. Dimova, V. A. Frolov, P. V. Bashkirov, H. Grubmüller, R. Jahn, H. J. Risselada *et al.*, *Journal of physics D: Applied physics*, 2018, **51**, 343001.
13 P. Rangamani, K. K. Mandadap and G. Oster, *Biophysical journal*, 2014, **107**, 751–762.
14 H. Alimohamadi and P. Rangamani, *Biomolecules*, 2018, **8**, 120.
15 Z. Lipatova, A. U. Hain, V. Y. Nazarko and N. Segev, *Critical reviews in biochemistry and molecular biology*, 2015, **50**, 203–211.
16 D. H. Murray, M. Jahnel, J. Lauer, M. J. Avellaneda, N. Brouilly, A. Cezanne, H. Morales-Navarrete, E. D. Perini, C. Ferguson, A. N. Lupas *et al.*, *Nature*, 2016, **537**, 107–111.
17 A. Singh, J. A. Soler, J. Lauer, S. W. Grill, M. Jahnel, M. Zerial and S. Thutupalli, *Nature Physics*, 2023, **19**, 1185–1192.
18 P. Y. P. Cheung, C. Limouse, H. Mabuchi and S. R. Pfeffer, *Elife*, 2015, **4**, e12790.
19 J. M. Wilson, M. De Hoop, N. Zorzi, B.-H. Toh, C. G. Dotti and R. G. Parton, *Molecular biology of the cell*, 2000, **11**, 2657–2671.
20 O. Kratky and G. Porod, *Recueil des Travaux Chimiques des Pays-Bas*, 1949, **68**, 1106–1122.
21 N. Saitô, K. Takahashi and Y. Yunoki, *Journal of the Physical Society of Japan*, 1967, **22**, 219–226.
22 G. Fredrickson, *The equilibrium theory of inhomogeneous polymers*, Oxford University Press, 2006.
23 W. Maier and A. Saupe, *Journal for Natural Research A*, 1958, **13**, 564–566.
24 W. Maier and A. Saupe, *Zeitschrift für Naturforschung A*, 1959, **14**, 882–889.
25 A. Ghosh, Q. MacPherson, Z.-G. Wang and A. J. Spakowitz, *The Journal of Chemical Physics*, 2022, **157**, 154906.
26 M. Doi and S. F. Edwards, *The theory of polymer dynamics*, oxford university press, 1988, vol. 73.
27 P.-G. De Gennes and J. Prost, *The physics of liquid crystals*, Oxford university press, 1993.
28 M. A. Blanco, M. Flórez and M. Bermejo, *Journal of Molecular structure: THEOCHEM*, 1997, **419**, 19–27.
29 A. J. Spakowitz and Z.-G. Wang, *The Journal of Chemical Physics*, 2003, **119**, 13113–13128.

30 F. C. Frank, *Discussions of the Faraday Society*, 1958, **25**, 19–28.
31 R. G. Priest, *Physical Review A*, 1973, **7**, 720.
32 W. Helfrich, *Zeitschrift für Naturforschung c*, 1973, **28**, 693–703.
33 P. B. Canham, *Journal of theoretical biology*, 1970, **26**, 61–81.
34 S. H. Mazharimousavi, S. D. Forghani and S. N. Abtahi, *International Journal of Geometric Methods in Modern Physics*, 2017, **14**, 1750062.
35 M. M. Terzi, M. F. Ergüder and M. Deserno, *The Journal of chemical physics*, 2019, **151**, 164108.
36 S. C. Takatori and A. Sahu, *Physical Review Letters*, 2020, **124**, 158102.
37 K. Sapp and L. Maibaum, *Physical Review E*, 2016, **94**, 052414.
38 J. J. Dumas, E. Merithew, E. Sudharshan, D. Rajamani, S. Hayes, D. Lawe, S. Corvera and D. G. Lambright, *Molecular cell*, 2001, **8**, 947–958.
39 T. Ohya, M. Miaczynska, Ü. Coskun, B. Lommer, A. Runge, D. Drechsel, Y. Kalaidzidis and M. Zerial, *Nature*, 2009, **459**, 1091–1097.
40 J. Faucon, M. Mitov, P. Méléard, I. Bivas and P. Bothorel, *Journal de Physique*, 1989, **50**, 2389–2414.
41 A. J. Spakowitz and Z.-G. Wang, *Macromolecules*, 2004, **37**, 5814–5823.